



Sangita Swapnasrita, Georg R. Pesch, Jochen A.H. Dreyer, Norbert Riefler, Thomas Wriedt, Lutz Mädler

Implementation of parcel method for surface reactions in DSMC

Journal Article as: peer-reviewed accepted version (Postprint)

DOI of this document* (secondary publication): <https://doi.org/10.26092/elib/2474>

Publication date of this document: 22/09/2023

* for better findability or for reliable citation

Recommended Citation (primary publication/Version of Record) incl. DOI:

Sangita Swapnasrita, Georg R. Pesch, Jochen A.H. Dreyer, Norbert Riefler, Thomas Wriedt, Lutz Mädler,
Implementation of parcel method for surface reactions in DSMC,
Computers & Fluids, Volume 187, 2019, Pages 1-11, ISSN 0045-7930,
<https://doi.org/10.1016/j.compfluid.2019.04.015>

Please note that the version of this document may differ from the final published version (Version of Record/primary publication) in terms of copy-editing, pagination, publication date and DOI. Please cite the version that you actually used. Before citing, you are also advised to check the publisher's website for any subsequent corrections or retractions (see also <https://retractionwatch.com/>).

This document is made available under a Creative Commons licence.

The license information is available online: <https://creativecommons.org/licenses/by-nc-nd/4.0/>

Take down policy

If you believe that this document or any material on this site infringes copyright, please contact publizieren@suub.uni-bremen.de with full details and we will remove access to the material.

Implementation of parcel method for surface reactions in DSMC

Sangita Swapnasrita^{a,d}, Georg R. Pesch^{b,d}, Jochen A.H. Dreyer^c, Norbert Riefler^a,
Thomas Wriedt^{a,d}, Lutz Mädler^{a,d,*}

^a Leibniz Institute for Materials Engineering IWT, Badgasteiner Straße 3, 28359 Bremen, Germany

^b Center for Environmental Research and Sustainable Technology (UFT), Leobener str. 6, 28359 Bremen, Germany

^c Department of Chemical Engineering and Biotechnology, University of Cambridge, United Kingdom

^d University of Bremen, Faculty of Production Engineering, Badgasteiner Str. 1, 28359 Bremen, Germany

ARTICLE INFO

Article history:

Received 4 December 2018

Revised 22 March 2019

Accepted 23 April 2019

Available online 23 April 2019

Keywords:

CO oxidation

Multi-scale modelling

Mesoporous layer

ABSTRACT

The parcel concept in Direct Simulation Monte Carlo method has been added to the reaction algorithm to the DSMC solver in OpenFOAM to reduce computational demand. Parcel per cell is checked for different cell sizes and different parcel sizes to obtain the right cell size for a given system. At this cell size, diffusion of CO in O₂ is simulated in a porous structure to ascertain the feasibility of this concept. After adding adsorption and reaction models, concentration profiles are obtained for different temperatures and different time steps. These profiles are compared with the single molecule algorithm written by Pesch et al. [14]. The local surface coverages and reaction rates are evaluated at a parcel size ranging from 10 to 100 to further validate the new approach. Computational time demand reduces by half at maximum parcel size to reach similar steady state results as that of the single molecule approach.

© 2019 Elsevier Ltd. All rights reserved.

1. Introduction

Mesoporous catalysts allow for efficient heterogeneous reactions to occur at their accessible active sites at the surface. The pore network can also provide support for surface functionalization. This accessibility helps increasing mass transfer rates for catalysed reactions, especially for gaseous reactants and products [1].

The Boltzmann and Navier Stokes equations are the traditional mathematical models for gas transport in such systems [2]. Rarefaction effects in these systems start where the mean free path of the gas is in the same order as the pore size of the catalyst, i.e., when the Knudsen number is smaller than the lower limit of the collisionless flow regime ($Kn \geq 3$) but larger than the upper limit of the transition regime ($0.001 < Kn < 0.1$). In this regime, the Boltzmann equation replaces the traditional continuum Navier-Stokes equation as the continuum gas dynamics assumption fails. A number of simulation techniques are readily available to model gas flows, e.g., lattice Boltzmann (LB), molecular dynamics (MD), kinetic Monte Carlo (KMC) or the dusty gas model (DGM). LB is a continuum approach based numerical method used for complex geometries. However, it is unsuitable for finding fundamental physical properties at mesoscopic scales [3]. At atomistic scales, MD

can be readily used for dense gases also. However, the fixed one-to-one correspondence in MD leads to computationally inefficient systems. Even now, researchers use only thousands of molecules to have reasonable computational expense [4,5]. It can only be used within small spatial regions and for short simulated periods. DGM is a transport model for gases through porous media based on Fick's law [6]. However, the simulated porous media is unrealistically considered as a stationary phase of dust particle. It is also limited to only homogeneous layers and a lot of computational workload is required to obtain structural information needed for the simulation. The Monte Carlo methods are based on a randomisation approach for deterministic problems. KMC is one such method to model gas flows with reactions. However, the prerequisite of this method is the definition of an accurate rate catalog which is often difficult to realize because of the many reaction pathways that can occur as a system evolves [7]. Direct Simulation Monte Carlo (DSMC), also based on MC, is a multiscale framework for coupling meso and macroscales and can be used to track molecules (in less detail compared to MD) while providing a good compromise for the computational time requirement and accuracy. It has no requirement of excessive structural information like pore diameter, porosity or tortuosity needed for DGM.

DSMC, a simulation method based on solutions of the Boltzmann equation, can be conveniently used to statistically simulate dilute gases, where the mean free path is greater than the characteristic length such that $Kn > 1$ [2,8]. The probabilistic approach is also convenient to decouple the molecular motion and

* Corresponding author at: Department of Production Engineering, Badgasteinerstrasse 3, 28355 Bremen, Germany.

E-mail address: lmaedler@iwt.uni-bremen.de (L. Mädler).

intermolecular collision over short intervals of time as the collisions are calculated based on statistics rather than individual tracking of molecules. DSMC has been consistently used to model molecular simulations for rarefied gas flows [9–10], hypersonic flows [11], spacecraft reentry [12], rarefied gas dynamics in mesoporous structures [13,14] and heat transfer in micro-channels [15,16]. The considered number of molecules can vary in a wide range from less than 10^3 [8] to an order of 10^{23} [9]. If the number of molecules is large, it is more efficient to use *parcels* as a representative molecule to reduce the computational demand in DSMC. Each simulated molecule, i.e. a *parcel*, would represent n real molecules. The collision probability is adjusted accordingly and the approach helps to reduce the computational effort without compromising the simulation accuracy. Due to the stochastic nature of DSMC, statistical noise can become significant if the number of considered parcels is reduced too much. These fluctuations are generally reduced when properties are averaged over time. The DSMC procedure can also be modified to introduce chemical reaction to the model.

Our main interest lies in gas diffusion and reactions within mesoporous layers in gas sensors, catalysts and air batteries. When the gas diffuses through these layers, it interacts with the mesoporous structures by adsorption on surfaces and reaction with other molecules, which can be simulated using DSMC. Dreyer et al. and Pesch et al. have simulated gas diffusion and reactions in mesoporous structures using the DSMC procedure but only for single molecules which is a parcel size of $n=1$ [13,14]. However, the simulation of heterogeneous surface reactions at a molecular level requires large computational time.

This paper proposes a modification of the DSMC routine of Pesch et al. [14] that simulates heterogeneously catalyzed surface reactions for a parcel size of $n=1$ to include larger parcel sizes and thus reduces the computational demand. For this purpose, the parcel method is first used for gas diffusion to see the extent of concentration profile deviations for different parcel sizes and also different cell sizes. The adsorption and reaction model are then added to diffusion for further analysis of the dependence of certain physical quantities, i.e., reaction rate, surface coverage on the parcel size. All the results from Pesch et al. are reproduced to check the validity and consider the error from the use of the parcel method.

2. Methods

The structure of highly porous layers for gas sensors as produced by flame spray pyrolysis have been simulated earlier [17,18]. For the computation, the porous layers are formed by Brownian transport of nanoparticle agglomerates. The porosity is 93% and the pore sizes range from 8 to 110 nm. Further information on pore characteristics can be found elsewhere [13]. In the current work, a simulation cuboid with a dimension of 1000 nm in x -direction and 240 nm in the y and z -direction is used with a resolution of cells of 8 nm cubic dimension (see supplementary S4). A reflecting wall is placed at the end of $x=1000$ nm representing the wall of the reactor or gas sensor electrodes [13,14]. The molecules initial positions are randomly chosen at $t=0$ and every time step Δt they are displaced following Newton's laws of motion

$$r_i^{t+\Delta t} = r_i^t + \Delta t * v_i \quad (1)$$

where r_i^t is the position vector at time t and v_i is the velocity vector of the particle i .

Following this, a pair of molecules in each cell is randomly sampled for the probability of collision (using no-time counter method as discussed later) irrespective of the exact position of the molecule. If the collision is accepted (upon comparison with a random number), the pre-collision velocities are replaced by post-collision velocities. Various molecular models such as

hard sphere, variable hard sphere, variable soft sphere, or square well model were designed to calculate collision probabilities and post-collision velocities. To study the fundamentals of such mechanisms, Dreyer et al. implemented the variable soft sphere model in DSMC to simulate gas diffusion in mesoporous structures [13]. This model was further used by Pesch et al. to include molecular adsorption of CO and dissociative adsorption of O₂ (also based on random probabilities which are discussed later) and surface reactions for CO oxidation on a pure palladium mesoporous layer under atmospheric pressure [14]. Pesch and Dreyer considered single molecules, i.e., a parcel size of $n=1$ (each real molecule is represented by one simulated molecule) for their DSMC simulations in OpenFOAM. The reaction mechanism is described by the Langmuir–Hinshelwood reaction model. Both reactants need to be present on the surface for the possibility of a reaction to take place. The product CO₂ is weakly bound to the catalyst surface and CO₂ surface lifetime is quite short above 100 K [19,20]. So, the reaction step in this mechanism is irreversible and CO₂ desorbs as soon as it is formed. All the probabilities involved in this simulation refer to the simple probabilistic approach of Monte Carlo. In case of adsorption, molecules which are rejected (probability of the event happening is smaller than a random number) are added back to the gas phase. However, in case of parcels, a definite number of molecules represent one parcel and the molecules of the parcel that are rejected are insufficient to form a new parcel in the gas phase because the parcel size is fixed. Hence, it is necessary to track rejected molecules from parcels with a list (*floating molecules list*) to maintain mass balance in the system. This is also true for desorption and reaction if the number of locally desorbing molecules is different to the required amount to form a parcel.

2.1. Floating molecules list

The floating molecules list stores the molecules that were randomly unaccepted during adsorption at a certain point of the simulation. All the molecules that are desorbed are also added to the list. Basically, the floating molecules list contains molecules that are not adsorbed on the catalyst surface and are desorbed to the gas phase. It is a non-physical entity that holds all the rejected and desorbed molecules at this time interval. This list is accessed at the end of each time step to count the number of accumulated molecules regardless of its origin from adsorption, desorption or reaction, only depending on the species of the molecule. Once the required molecule number is reached at a particular surface, one parcel is added back to the gas phase into the cell adjacent to that surface (see Fig. 1, Initialisation). This introduces a general time lag from the moment a molecule is rejected/desorbed to the time it is added back to the gas phase. The time lag increases as the parcel size is increased. However, when steady state is reached, a balance is achieved between the adsorbed, gas-phase and floating molecules and the final gas phase concentration profiles remain similar.

2.2. Simulation set-up

The inlet for the gas also acts as an outlet and is positioned opposite the reflecting wall ($x=0$ nm). Cyclic boundary conditions are used for the other walls. Pure palladium is considered for the nanostructured layers and all the simulation parameters are obtained from experimental literature values of oxidation of CO on Pd(111) surfaces under ultrahigh vacuum conditions [2,19–24,26–33]. Although their adaptation to atmospheric conditions may not be fully accurate, the results are physically descriptive and can be understood at a fundamental level. Theoretical and experimental results are used to derive the simulation parameters based on a simplified isothermal reactor approach. Although the system is not

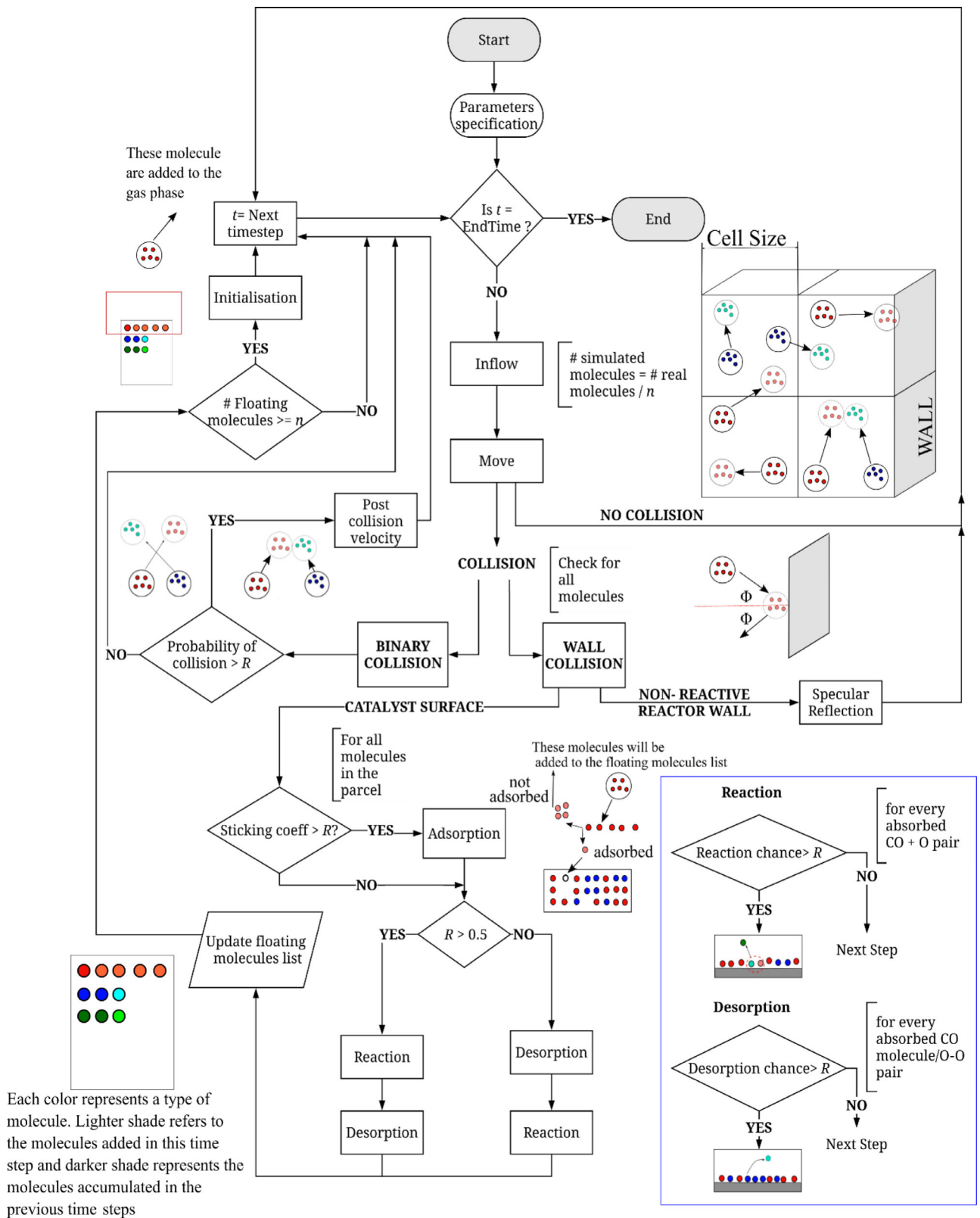


Fig. 1. Flow chart illustrating the steps involved in the parcel method ($n=5$ for illustration purposes) used in the paper. Individual steps are discussed in the text in the order of their occurrence. R refers to a newly generated random number between 0 and 1 for each new step.

thermodynamically conserved, the influence of temperature on the microkinetic framework is considered as parameters are temperature dependent.

In the DSMC reaction model developed by Pesch et al. single molecules diffuse through the porous layers and meanwhile get adsorbed on the vacant sites and react. While diffusing within pores, the molecules are also involved in molecular collisions. In the reaction step, adsorbed CO and O irreversibly react to form CO₂, which then immediately desorbs into the gas phase. Indexing and tracking of each individual molecule leads to an increase in computational time as the computational probability needs to be calculated for each molecule to obtain the new deflection angles and velocities. Thus, Bird [2] incorporated the parcel method in his DSMC formalism for gas diffusion processes. In the DSMC method, simulated molecules can represent n number of real molecules, n being any positive integer. These simulated molecules are designated as parcels to avoid confusion. When the parcel size is very high, it helps in reducing computational expenses. In this work, parcel sizes in the range of 1–100 have been used to simulate catalytic reactions. The DSMC reaction solver used by Pesch (2015) had to be adapted for the parcel method. In the following section, the different steps involved in Pesch's DSMC simulation as shown schematically in Fig. 1 and the required modifications to include parcels are discussed in detail.

2.3. Collision sampling

According to the probabilistic approach of DSMC, the parcels are moved in random directions. Thus, it may occur that parcels are superimposed or are in the vicinity of other parcels. This occurrence could lead to "collision" equivalent to binary collision in real gases. Collision may also occur between a parcel and a wall, wall being either the catalyst surface or the reflecting walls of the simulation box.

In a DSMC solver, the computational domain is divided into a finite number of mesh cells [2]. Collisions between two parcels i and j may occur if both are located inside one cell independent of their exact location based on the collision probability calculated by NTC (no-time-counter) scheme proposed by Bird [2,25]. It is an efficient version of the TC (time-counter) method also proposed by Bird [25].

The collision probability is calculated for a set of $\frac{1}{2}N\bar{N}n(\sigma_{TCr})_{max}\Delta t/V_C$ pairs of molecules at a probability of $\frac{\sigma_{TCr}}{(\sigma_{TCr})_{max}}$ which is the volume swept by the two colliding molecules during Δt both normalized by the maximum value of σ_{TCr} possible. This is done to reduce the error for small values of N at large values of n to include only a fraction of colliding pairs and the probability increased by the same fraction.

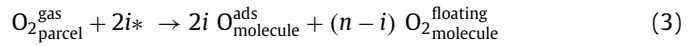
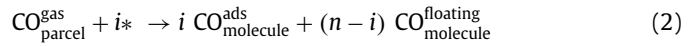
The average number of parcels N given for a number density η of molecules in a cell volume V_C , where each parcel contains n real molecules, is given by $\eta V_C/n$. The number of pairs in the cell is given by $(\frac{1}{2}N\bar{N})$ where N is the instantaneous average value and \bar{N} is the time or ensemble averaged value. The value of the volume swept by the total cross section σ_{TCr} of two colliding parcels moving at their relative velocity c_r is given by $n\sigma_{TCr}\Delta t$. In the case of gas mixtures composed of molecules with similar masses, as in this work, all molecular groups are considered as single species neglecting the slightly higher value of σ_{TCr} for lighter molecules. Lighter molecules would have higher relative velocities. And that would set the value for maximum σ_{TCr} . So, the collision that heavy molecules would be selected will be lower. Collision cross sections for parcels is calculated by $\sigma_{real\ molecule} * \frac{\text{number of real molecules}}{\text{number of parcels}}$, thus maintaining the right collision probabilities. This weighted cross-section method conserves both mass and energy in the system. Post-collision velocities are calculated based on Variable Soft

Sphere model proposed by Bird [2]. In case of a collision with a "wall", parcels undergo specular reflection from the surfaces which means they have a direct elastic collision with the wall.

2.4. Adsorption mechanism

The surface mechanisms for adsorption written for single molecules were implemented by Pesch et al. [14]. In Pesch's work, individual molecules were adsorbed on the surface depending on the surface sticking coefficient. The challenge faced when including parcels is how to accommodate parcels on the adsorption sites of each face if each face has a certain maximum surface coverage for CO and O. If the entire parcel were accommodated on the surface, it could lead to overcrowding of the surface and if only a random fraction of molecule is adsorbed, then the rest of the parcel is lost as it no longer counts as one parcel.

Our approach is to use the *floating molecules* list. Adsorption and reaction steps are still resolved at a molecular level. When a parcel reaches a surface, all n molecules in the parcel have a chance for adsorption depending on the sticking coefficient and the surface coverage of the face. As the surface coverage increases, the sticking coefficient reduces and thus the probability of further adsorption of molecules decreases. After all the molecules are sorted, the parcel is subsequently deleted from the gas composition. The next molecule that reaches the surface also proceeds through the same steps with the updated coverage and sticking probability. All the unaccepted molecules that belong to the parcel are then written in the *floating molecules* list.



where i is the number of adsorbed molecule.

Physically, there is competitive adsorption of CO and O₂ on the free surface sites (*). This competitive nature of adsorption is taken into account in Pesch's work by modifying the θ for both gases as follows [14],

$$\theta_{\text{req,CO}} = \frac{\theta_{\text{max,CO}} - \theta_{\text{CO}}}{\theta_{\text{max,CO}}} \quad (4)$$

$$\theta_{\text{req,O}} = \left(1 - \frac{\theta_{\text{O}}}{\theta_{\text{max,O}}} - \frac{\theta_{\text{CO}}}{\theta_{\text{max,CO}}}\right)^2 \quad (5)$$

The variable θ_{req} is the probability to find the required number of vacant surface sites, θ_{max} is the number of available adsorption sites, divided by the maximum surface coverage from literature. In this work, a value of $\frac{1}{3}$ for CO and $\frac{1}{4}$ for O₂ was chosen from the molecular beam experiments [26–28] as explained in Pesch's work [14]. The adsorption probability is expressed in terms of the sticking coefficient, which is the probability of a single molecule to adsorb on the surface as a function of surface coverage. In this work the sticking coefficient, S , is derived from the Kisluik model [29,30] for precursor mediated adsorption,

$$S(\theta) = S_0 \left(1 + K \left(\frac{1}{\theta_{\text{req}}} - 1\right)\right)^{-1} \quad (6)$$

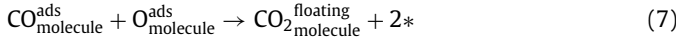
The initial sticking coefficient S_0 and the prefactor K are fitted to experimental data from $S(\theta)$ curves (as explained by Pesch et al.). For CO and O₂, S_0 values are determined as 1 and 0.60 while temperature dependent K values are fixed at 0.15 and 0.71, respectively.

At every time step, for every parcel that reaches the nanoparticle surface, $S(\theta)$ is compared to a random number R . The first molecule of the parcel adsorbs if $S(\theta) > R$. The coverage is updated accordingly. The subsequent molecules' adsorption is then

dependent on the sticking coefficient calculated from the updated θ values. This loop continues for all the molecules in the parcel (Fig. 1). The number of molecules that are accepted in this step gives us the number i used in Eqs. (2) and (3). After adsorption of any molecule, it can either desorb from the surface or react with adjacent molecule depending on the corresponding surface coverage. To determine the sequence of this desorption/reaction process, a random number is compared to 0.5 (see Fig. 1).

2.5. Reaction mechanism

The Langmuir Hinshelwood mechanism is considered for CO oxidation as in the original work of Pesch et al. [14]. CO oxidation would proceed by an irreversible reaction between adjacently adsorbed CO and O.



The surface free sites are represented by $*$.

The Langmuir Hinshelwood reaction rate for CO_2 formation is given by an Arrhenius-type equation

$$r_{\text{CO}_2} = \nu_{\text{LH}} f(\sigma_{\text{CO}}, \sigma_{\text{O}}) \exp\left(-\frac{E_{\text{LH}}}{RT}\right) \quad (8)$$

which accounts for temperature dependence by the activation energy E_{LH} . The reaction rate depends on the pre-exponential factor, $\nu_{\text{LH}} = 2.5 \times 10^{-3} \text{ cm}^2 \text{ s}^{-1}$, and the surface coverage of both the gas molecules. The function f takes into account, how the molecules are distributed over the surface. If the coverages are low and the molecules are randomly distributed on the surface, then $f = \theta_{\text{CO}}\theta_{\text{O}}$, which is a second order reaction and what is assumed in this work. The E_{LH} value is taken from literature for CO oxidation as 84 kJ/mol [32]. The reaction probability is decided by the ratio of the reaction rate and the surface coverage per area of the particles, $P_{\text{reac}} = r_{\text{CO}_2} \frac{\Delta t}{\sigma}$. After comparing this reaction chance to a random number, CO_2 that is formed is added into the *floating molecule* list rather than the gas phase as in the case of single molecule parcels (Fig. 1). This is done to ensure that only parcels of size n are initialised into the gas phase. The volume averaged reaction rate is represented by r_{LH} and is used to determine an overall steady state for the oxidation reaction.

2.6. Desorption mechanism

Desorption mechanism is modelled according to the Polanyi-Wigner equation [19],

$$r_{\text{des}} = \nu_{\text{des}} \theta^k \exp\left(-\frac{E_{\text{des}}}{RT}\right), \quad (9)$$

where r_{des} is the rate of desorption which is exponentially related to desorption activation energy E_{des} and absolute temperature T , ν_{des} is the pre-exponential factor and the desorption order, k is 1 for the molecular desorption of CO and 2 for the associative desorption of O_2 . The values of E_{des} and ν_{des} for CO and O_2 are taken from Refs. [26] and [33] respectively.

In most cases, the pre-exponential factor depends on the coverage θ and can be expressed by $\nu_{\text{des}} = 10^{c_a + c_b \theta}$ with the fitting parameters c_a and c_b [14]. E_{des} also depends on the coverage

$$E_{\text{des}} = E_{\text{des}}(0) + \theta \times E_{\text{des, lateral}} \quad (10)$$

where $E_{\text{des}}(0)$ is the desorption energy at zero coverage, $E_{\text{des, lateral}}$ is the energy term describing lateral molecular interactions (either weakening or intensifying of the adsorption bonds), given by $E_{\text{des, lateral}} \times \theta_{\text{max}} = \omega_{\text{pair}} \times N_{\text{nearest}}$, θ_{max} is the maximum surface coverage, N_{nearest} is the number of nearest neighbours and ω_{pair} is the interaction potential between them.

The probability of the desorption step is

$$P_{\text{des}} = \frac{r_{\text{des}} \Delta t}{\sigma} \quad (11)$$

where $\sigma = \frac{N_{\text{ads}}}{N}$ is the density of the species on the surface. If $P_{\text{des}} > R$, the molecule desorbs. The algorithm removes this molecule from the adsorption list and adds it to the *floating molecules* list of this molecule. When desorption takes place, the surface coverage is updated before iterating for the next time step.

2.7. Initialisation from floating molecules list

The gas phase steps such as binary collision, wall collision and movement are performed for parcels. In the other steps involving the catalyst surface, the molecules which are rejected from adsorption or newly produced CO_2 molecules or the molecules from desorption are added into a *floating molecules* list for a particular surface. At the end of each time step, the *floating molecules* list for each species needs to be checked for sufficient molecules to initialise a parcel into the gas phase. Every time step, when the number of *floating molecules* on a face exceeds the parcel size n , one parcel is initialised into the gas phase and n molecules are deleted from the list. Excess *floating molecules* are retained in the list for the next time step. This initialised parcel is randomly allocated a position inside the cell corresponding to the surface in consideration and a random Gaussian velocity based on the isothermal temperature of the system.

3. Results and discussion

The following discussion compares the parcel method with the single molecule method in terms of similarity of results and computational time required to simulate on 10 processors of a 12 core Xeon server (2.7 GHz, 40GB RAM). The simulations are continued (for a time step of 5 ps) until steady state is achieved in all cases.

3.1. Diffusion only

To investigate the influence of parcel size n and cell size (thus, the amount of parcels per cell) on the gas diffusion, the diffusion of 10% CO and 90% O_2 is investigated first in an empty cuboid (no porous structure is involved) filled with O_2 at 1 atm. The inlet gas diffuses through the simulation volume at 323 K and atmospheric pressure. The case is divided into two sub-cases: (1) keeping n fixed, cell size is varied, (2) keeping cell size fixed, n is varied (all parameters for sub-cases are given in Table 1) and (3) same as (2) but with a porous structure of same dimensions and 93% porosity.

For all cases, the cuboid is divided into 10 nm slices in x -direction to calculate the CO concentration as function of x and time t . The dependence of CO concentration on cell size and parcel size was evaluated to find the limits of the parcel method and to maximise the computational efficiency.

Sub-case 1: In an empty cuboid, n is fixed at 1 so that each simulated parcel represents one real gas molecule and the cell sizes are varied between 2 and 20 nm to obtain different parcel per cell (PPC) values. Low PPC values have posed a problem in some of

Table 1
Sub-cases for CO diffusion simulations inside an empty cuboid.

	Parcel size (n)	Cell size (nm)
Sub-case 1	1	2, 4, 8, 10, 20
Sub-case 2	1, 10, 20, 50, 100	8
Sub-case 3 (with porous layer)	1, 10, 20, 50, 100	8

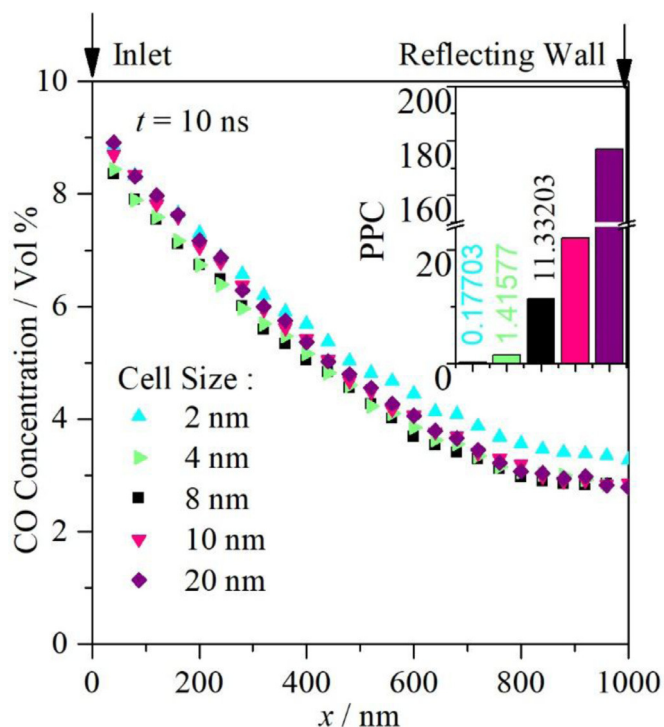


Fig. 2. CO gas concentration for $n=1$ using different cubic cell sizes. Inset: Number of parcels per cell (PPC) for the considered cases.

the past studies when, for example, the parcel per cell went below 5 for a case with Poiseuille flow in slip and transition regime because of inaccurate collision predictions [34].

Similar concentration profiles with an exponential decay are observed for the different cell sizes. The rate of diffusion is slightly overestimated if 2 nm cells are used and PPC drops below 1 (Fig. 2). With decreasing cell size, the computational time increases substantially (almost 5 fold from 2 nm to 8 nm, Supplementary figure S1). The computational time remains invariable when the cell size is increased beyond 8 nm.

Sub-case 2: Another way to reduce computational time is to increase the parcel size. The effect of parcel size was studied here using fixed cell size of 8 nm. 8 nm cubes have equivalent volume of 10 nm spheres. Thus, they can be used to model the porous structure, used in this study, which was formed by 10 nm spheres [13]. The CO gas concentration profile in an empty cuboid for a fixed cell size of 8 nm is shown in Fig. 3a.

The gas concentrations are shown for cell size of 8 nm and a wider range of parcel size could be used to get similar concentration profiles. In the inset, we see the parcel per cell values as n is increased. PPC value for $n=100$ is 0.15 and that for $n=50$ is 0.30. The corresponding concentration profiles show that fluctuations are visibly more pronounced when PPC drops below 0.2.

Sub-case 3: The diffusion process is different when the molecules interact with a porous structure rather than an empty cuboid. So in the next step, the CO gas concentration profiles in a porous structure of similar dimension of sub-case 2 for a fixed cell size of 8 nm are shown in Fig. 3b. The data is fitted by an analytical solution for diffusion in porous structure for a porosity of 93% and effective diffusion coefficient $1.1 \times 10^{-5} \text{ m}^2 \text{ s}^{-1}$.

The rate of diffusion is lower in a porous structure because of more parcel-wall interactions compared to an empty cuboid. The deviation is also less prominent in a porous structure than in an empty cuboid. It can be argued that in porous structures as in this case, the pore size is small resulting in more collisions (Supple-

mentary figure S2). The fluctuations are also dependent on PPC as shown earlier. It can be inferred that there is a need to maintain PPC in the cell to reduce large fluctuations in the properties. That threshold value is 0.2 in this work, different from a value of 5 which was suggested in earlier studies [34]. The structure with 8 nm has a PPC of about 12 at $n=1$ (Fig. 3) and just below 0.2 for $n=100$. At this particular cell size the computational time reduces by a factor of 26 when the parcel size, n is increased from 1 to 100 (see later Fig. 11).

3.2. Diffusion with adsorption

The next step towards a reaction model is to add the possibilities for the molecules to adsorb on the vacant surface sites while diffusing through the porous structure. Again, 10% CO is introduced into the simulation volume saturated with O_2 . However, in this case CO may adsorb as it collides with the nanoparticle surface. It takes longer simulation time to achieve steady state as adsorption becomes the rate limiting mechanism. Even after 600 ns CO molecules have penetrated only 400 nm along x -direction into the reaction volume (Fig. 4). Most CO molecules tend to adsorb on the vacant sites rather than diffuse through the porous structure thus reducing the extent of diffusion into the structure. With time, more molecules are added to the *floating molecules* list as the surfaces reach saturation. Hence, these molecules are unavailable from the gas phase. Thus, larger fluctuations are observed when parcel size is increased. The concentration varied on an square averaged error of 0.015%. So, it is possible to obtain reliable concentration profiles at larger parcel sizes n . Additionally, the computational time reduces by a factor of 14 from 46,015 s at $n=1$ to 3208 s at $n=100$ (see later Fig. 11).

3.3. Oxidation of CO in the porous layers

In the next stage, reactions are considered using the Langmuir Hinshelwood reaction mechanism described previously. Molecules of CO and O_2 compete for adsorption on vacant sites on the particle surface. Adjacent CO and O_2 react to form CO_2 . The mesoporous structured particle surface is first saturated with the maximum coverage for both CO and O_2 ($\sigma_{\text{maxCO}} = 4.06 \times 10^{14} \text{ molecules/cm}^2$ and $\sigma_{\text{maxO}_2} = 3.34 \times 10^{14} \text{ molecules/cm}^2$) to reach expected steady state and reduce computational effort. Here, the inlet gas composition is 1% CO and 99% O_2 at atmospheric pressure and the temperature is set at 723 K to ensure fast reaction rates.

3.3.1. Reaction rate as a function of time

The volume averaged Langmuir Hinshelwood reaction rate as a function of time at temperature 723 K is shown in Fig. 5. At 723 K, the reaction rate is rather high but the amount of CO_2 formed is insufficient to replenish the CO_2 diffusing out through the inlet. Since the simulation is started with maximum CO and O coverages, the local surface coverage decreases and the reaction rate uniformly decreases until an adsorption-desorption-reaction equilibrium is reached. At about 8000 ns, the reaction rate barely changes and it can be assumed that an overall steady state is reached. This is in accordance to the conclusion of steady state by Pesch et al. [14]. The average reaction rate varies by about 2.6% for $n=100$ compared to $n=1$. This indicates that steady state conditions can be predicted for a reaction using parcel method at less computational cost.

3.3.2. Local surface coverage

The steady state surface coverages of CO and O_2 over the 1000 nm mesoporous layer are shown in Fig. 6. The O_2 surface coverage is zero near the inlet due to competitive adsorption by CO and its reaction to CO_2 but increases steadily to the maximum

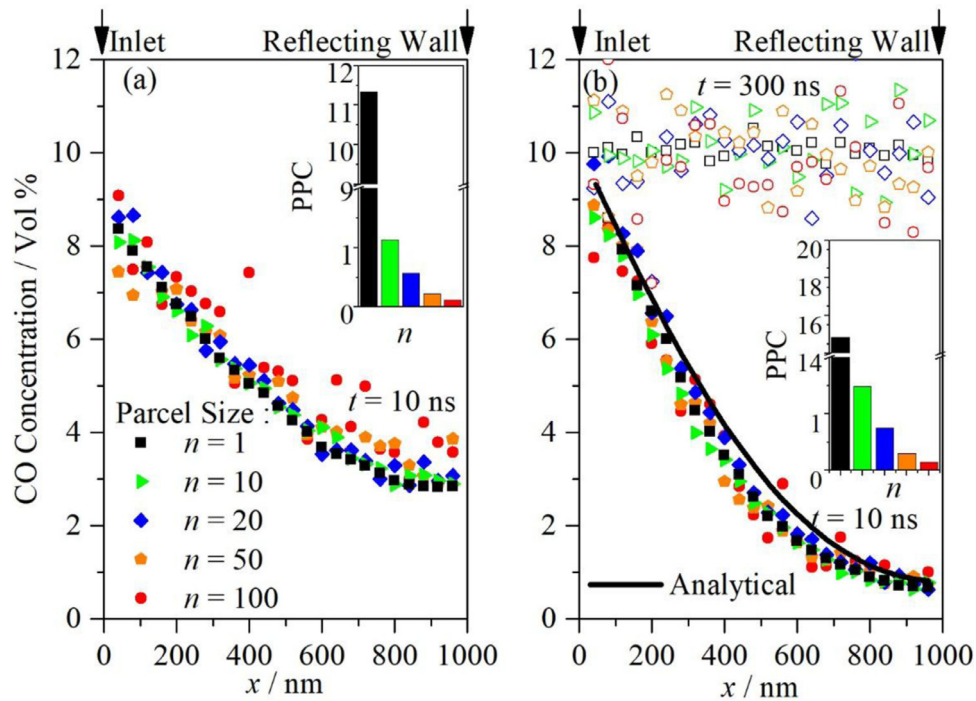


Fig. 3. Local CO concentration at different time steps for different parcel sizes in a) an empty cuboid b) porous structure. The solid line in figure b shows the analytical solution for diffusion in a porous structure. Both structures have same dimensions. CO diffuses in O_2 in a porous layer of 1000 nm length where $x=0$ nm represents inlet and $x=1000$ nm represents a reflecting wall. Insets show parcel per cell (PPC) in the simulation volume for different n .

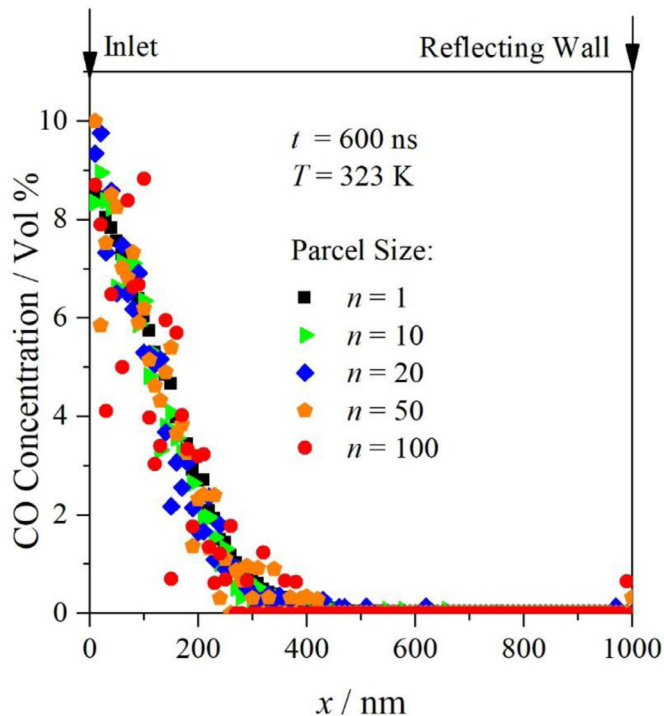


Fig. 4. Diffusion and Adsorption in porous structure. Local CO concentration at $t=600$ ns for different parcel sizes. Diffusion and adsorption of CO in O_2 in a porous Pd layer of 1000 nm length where $x=0$ nm represents inlet and $x=1000$ nm represents a reflecting wall.

value with increasing x . With increasing n , the onset of this increase in O surface coverage shifts closer to the inlet. The reason is that n molecules have a chance to adsorb on a surface when a parcel collides with a wall. Due to the higher O surface coverage,

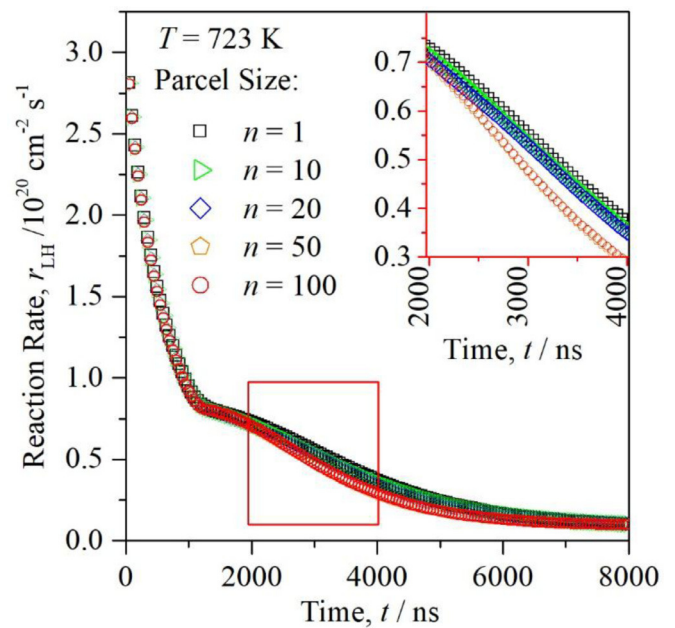


Fig. 5. Time distribution of reaction rate, r_{LH} during oxidation of CO in O_2 on a mesoporous Pd layer for different parcel sizes at 723 K. The inset shows $t=2000$ ns to 4000 ns in detail.

more oxygen is available to react with CO. Therefore, more CO can react and the CO surface coverage close to the inlet decreases with increasing n . Because of the preferential adsorption of CO over O_2 , the CO coverage close to the inlet is always higher than O. However, almost all CO adsorbs on the catalyst surface near the inlet or reacts to CO_2 , leaving the O surface coverage further inside the layer unchanged. Furthermore, this leads to a decrease in CO surface coverage (going close to zero) when approaching the reflecting

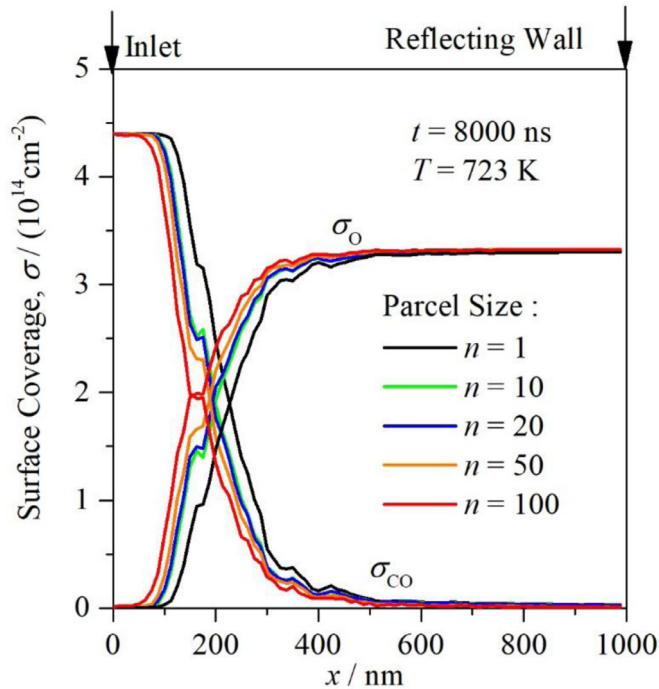


Fig. 6. Local surface coverage, σ_{CO} and σ_{O} at $t=8000$ ns for different parcel sizes. Steady state is assumed to be reached by this time.

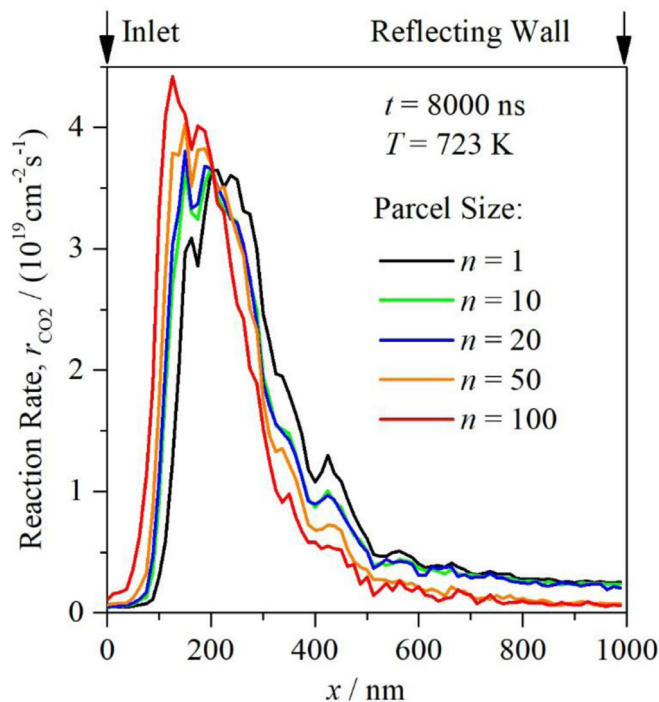


Fig. 7. Local reaction rate r_{CO_2} , at steady state $t=8000$ ns for different parcel sizes.

wall. The point where the O surface coverage exceeds to that of CO is referred to as the *surface coverage crossover point* and is between 130 and 200 nm. The local surface coverage with O and CO governs the local reaction rate, which is discussed in the next section.

3.3.3. Local reaction rate

The local reaction rate calculated from Eq. (8) is averaged over a 10 nm slices of the porous layers in the x -direction (Fig. 7). As seen in Fig. 6, the surface coverage crossover occurs earlier for in-

creasing parcel size. Because the CO_2 reaction rate uses the product of CO and O surface coverage (Eq. (8)), the maximum in the local surface reaction rate is observed at a similar location to the *surface coverage crossover point*. Consequently, the surface reaction rate shifts closer to the inlet with increasing parcel size n . Near the inlet where the surface is saturated with CO, no oxygen adsorption occurs and thus no CO oxidation is possible. Inside the porous layer, the oxygen surface coverage increases and the reaction rate starts increasing until it reaches a maximum. This maximum represents the reaction front of the catalyst (Supplementary S4). After the crossover, the CO coverage steadily decreases as it is used up in adsorption and reaction near the inlet. Hence, the reaction rate decreases to very low values towards the reflecting wall. As evident from Figs. 6 and 7, the local surface coverages and reaction rates show only a slight local deviation with increasing n , but the overall form of the curves is similar for all n .

3.3.4. CO_2 concentration

When considering only single molecules, the CO_2 molecule is desorbed instantaneously into the gas phase after reaction. In the parcel method, one CO_2 is added to the *floating molecules* list every time a reaction occurs. Every time step, the *floating molecules* lists are updated. If the number of molecules is greater than or equal to the parcel size n , one parcel is added to the gas phase composition (see Fig. 1). The CO_2 concentration produced from the reaction at different times can be seen in Fig. 8a. The CO_2 gas concentration profile becomes statistically noisy when the parcel size is increased as the averaging of properties is done for fewer parcels. There is no gas-phase CO_2 at $t=150$ ns for $n=50$ and 100. Thus, we averaged the CO_2 concentration for higher parcel sizes ($n=50$ and 100) over at least 3 runs (Fig. 8b). However, at time $t=2000$ ns, if we compare the unaveraged and averaged concentration for $n=50$, even though the fluctuations are minimized, there is a significant deviation from the other profiles. For $n=100$, there is still no gas phase concentration at $t=2000$ ns. This is due to a delay in initialisation of the parcels from the *floating molecules* list to the gas phase, i.e., the list must be filled with n molecules before a parcel can be initialised. It can also be observed that the gas concentration is low at the inlet ($x=0$) because it acts as open boundary and therefore CO_2 diffuses out of the cuboid. The figure shows that concentration can be very accurately predicted even as the parcel size is increased to 20. Beyond that, a large difference is observed in the predicted gas concentration (Fig. 8b). It should be noted that for parcel method, the molecules are saved in the *floating molecules* list until it is initialised. This observed difference should, by no means, be understood as a fault in the reaction rate prediction by the algorithm. Instead, it is the result of residual molecules left over from the previous time-steps being initialised at a later time (see Fig. 9). There is an increasing delay in the initialisation of the CO_2 from the *floating molecules* list as the parcel size increases. It takes longer simulation time to accumulate a higher parcel size on one surface and thus, parcels are introduced later to the gas phase. It can also be noted that concentration profiles are omitted for $n=100$ to keep the figure clear. The simulation computational time reduces by a factor of 2.5 when $n=100$ compared to $n=1$ (Fig. 11).

3.3.5. Arrhenius plots at $t=0$ and steady state

Arrhenius plots are drawn for different temperatures at $t=0$ and at steady state to supplement the validity of larger parcel size (Fig. 10). These plots are used to validate the activation energy for a particular reaction to occur and to study the rate limiting steps.

The simulations are initiated with maximum surface coverages of CO and O at $t=0$. At lower temperatures, the diffusion process

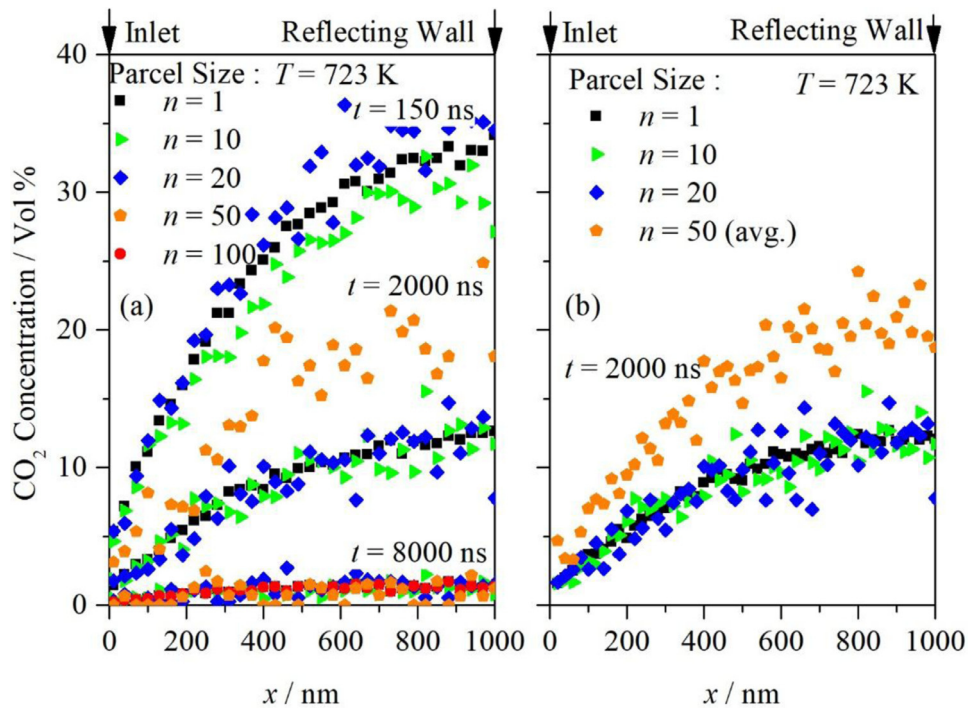


Fig. 8. Oxidation of CO in a porous structure. (a) Comparison of local gas-phase CO₂ concentration along the length of the porous Pd structure at $t = 150, 2000$ and 8000 ns. Different parcel sizes n are used. (b) CO₂ concentration curves for parcel size of 1, 10, 20 and 50 (averaged) respectively at $t = 2000$ ns.

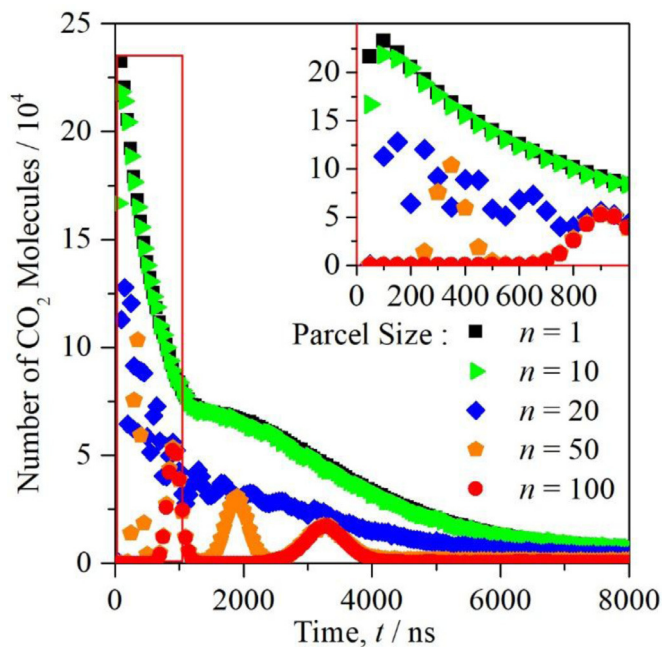


Fig. 9. Number of CO₂ molecules at different times for different n . The inset shows first 1000 ns in detail.

is sufficient to replenish the CO and O removed through CO oxidation and the reaction rate remains constant once steady state is reached. However, as the temperature increases, the reaction rate is larger than the rate of diffusion in the porous layer. So, there is a diffusion limit at higher temperatures when steady state is reached. The activation energy value from the plots agrees with the kinetic limit of the reaction ($83.68 \text{ kJ mol}^{-1}$) observed from the experiments of Engel et al. [20]. It can be argued that the differences in reaction rate are negligible for parcel sizes in between 1 and

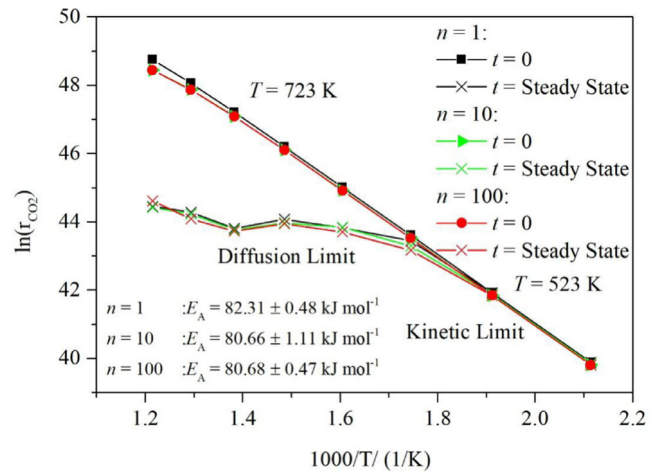


Fig. 10. Arrhenius plots for CO oxidation at different temperatures for time $t = 0$ and $t = \text{steady state}$.

100. Therefore, the reaction rate remains unaffected by the size of the parcel, both at initial and steady state.

4. Discussion

The parcel method implemented in the DSMC solver of OpenFOAM has been used for the complex molecular processes during CO oxidation in a mesoporous Pd layer. Previously, surface reactions were incorporated into DSMC by Pesch et al. for studying CO oxidation on pure Pd. Many fundamental descriptions are made to understand the local reaction rate, the surface coverage and CO₂ production at various temperatures and time. Steady state for such reaction is also discussed for different temperatures. In this work, the parcel method is used to reduce the computational demand. DSMC is based on simulated molecules (parcels), where

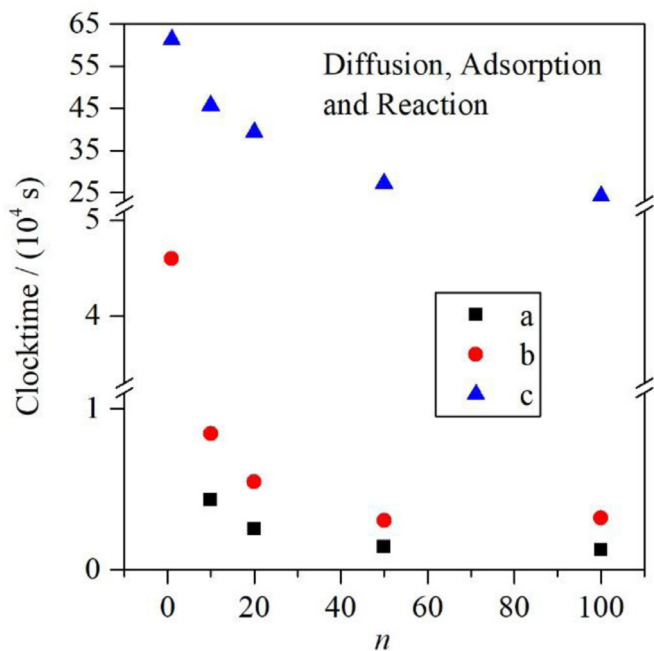


Fig. 11. Computational time for (a) Diffusion only, (b) Diffusion and adsorption and (c) Diffusion, adsorption and reaction for different n to reach steady state.

each parcel represents a number of real molecules. However, surface reactions using the parcel method have not been reported. At the cost of a slightly less statistically accurate results, similar gas phase concentration curves and volume averaged reaction rate profiles are obtained. Similar steady states achieved at various temperatures emphasise that the dependence of reaction rate on temperature is invariant of parcel size. The influence of cell size on the simulation results was also studied. As the cell size was reduced below 2 nm for a parcel size of 1, an over-estimation of diffusion rate was observed. While keeping the cell size constant, if the parcel size is increased, it leads to more scatter in the concentration curves. However, if the data was fitted by a suitable function, similar concentration curves were obtained. This scatter is also reduced by maintaining the number of parcels per cell above 0.2.

In this work, a floating molecules list is considered to hold all the molecules that are neither absorbed nor in the gas phase. This list is required for the conservation of mass and energy. However, the absence of these molecules from the gas phase causes inaccurate concentration predictions. It also causes the delay in the onset of CO₂ production as the parcel size is increased due to the time required to initialise a parcel of a particular size. Unless that parcel size is reached, the molecules are in the floating molecules list which implies they are absent in the gas phase concentration. For CO and O₂ molecules, this impedes their chance for readsorption after desorption. However, at the steady state time, the coverages, gas phase concentration and the floating molecules are in a balanced state for various parcel sizes and the average reaction rate remain constant throughout the mesoporous layer. It is also needed to address the delay at each time steps which could be done by implementing variable parcel sizes in DSMC solver which will be realized in future work.

Gas concentration profiles in cases of diffusion, diffusion with adsorption and no reaction and diffusion with adsorption and reaction remain similar as the parcel size is increased. This shows that the gas concentration at any particular point of the mesoporous structure can be predicted at less computational time. Further, a shift of maximum local reaction rate is observed as

the parcel size increases towards the inlet of the structure. An empirical correction to the adsorption coefficient depending on the parcel size can improve the adsorption profile but this correction is complex to realise in the scope of this work. However, even with the local shift, the determined steady state reaction rate remains constant which shows that the simulation predictions remain unchanged for increasing parcel size at near steady state conditions.

5. Conclusions

Oxidation of CO on pure Pd mesoporous layer at atmospheric pressures has been simulated using a parcel method with the DSMC solver in OpenFOAM. With an error of 2.6% when parcel size is increased from 1 to 100, similar steady state parameters could be predicted for CO oxidation in the porous Pd layer in less than half the time required for a single molecule approach. This approach can serve as a basis to develop models in the future which are more complex and realistic in nature.

Acknowledgements

The authors would like to thank the German Research Foundation (DFG) for support through the Research Training Group GRK 1860 "Micro-, meso- and macroporous nonmetallic Materials: Fundamentals and Applications" (MIMENIMA).

Declaration of interest

None.

Supplementary materials

Supplementary material associated with this article can be found, in the online version, at doi:10.1016/j.compfluid.2019.04.015.

References

- [1] Corma A. From microporous to mesoporous molecular sieve materials and their use in catalysis. *Chem Rev* 1997;97(6):2373–420.
- [2] Bird GA. *Molecular gas dynamics and the direct simulation of gas flows*. New York: Clarendon Press, Oxford University Press Inc; 1994.
- [3] Chen S, Wang M, Xia Z. Multiscale fluid mechanics and modelling. *Procedia IUTAM* 2014;10:100–14.
- [4] Alder BJ, Wainwright TE. Studies in molecular dynamics I. General method. *J Chem Phys* 1959;31(2):459–66.
- [5] Song Y, Xu F, Wei M, Wang Y. Water flow inside polyamide reverse osmosis membranes: a non-equilibrium molecular dynamics study. *J Phys Chem* 2017;121(7):1715–22.
- [6] Veldsink JW, van Damme RMJ, Versteeg GF, van Swaaij WPM. The use of dusty-gas model for the description of mass transport with chemical reaction in porous media. *Chem Eng J* 1995;57:115–25.
- [7] A.F. Voter, Introduction to the kinetic Monte Carlo method, in: K. E. Sickafus, E. A. Kotomin, B. P. Uberuaga (Eds.), *Radiation effects in solids: proceedings of the NATO advanced study institute, Erice, Sicily, Italy, July 17–29, 2004*, NATO science series, Springer, The Netherlands, p. 1–24.
- [8] Pavan V, Oxarango L. A new momentum equation for gas flow in porous media: the Klinkenberg effect seen through kinetic theory. *J Stat Phys* 2007;126(2):355–89.
- [9] Scanlon TJ, Roohi E, White C, Darbandi M, Reese JM. An open source, parallel DSMC code for rarefied gas flows in arbitrary geometries. *Comput Fluids* 2010;39(10):2078–89.
- [10] Alexander FJ, Garcia AL. The direct simulation Monte Carlo method. *Comput Phys* 1997;11(6):588–93.
- [11] Scanlon TJ, White C, Borg MK, Palharini RC, Farfar E, Boyd ID, Reese JM, Brown RE. Open-source direct simulation Monte Carlo chemistry modeling for hypersonic flows. *AIAA J* 2015;53(6):1670–80.
- [12] Moss JN, Bird GA. Direct simulation of transitional flow for hypersonic reentry conditions. *J Spacecr Rockets* 2003;40(5):830–43.
- [13] Dreyer JAH, Riefler N, Pesch GR, Karamehmedović M, Fritsching U, Teoh WY, Mädler L. Simulation of gas diffusion in highly porous nanostructures by direct simulation Monte Carlo. *Chem Eng Sci* 2014;105:69–76.
- [14] Pesch GR, Riefler N, Fritsching U, Ciacchi LC, Mädler L. Gas-solid catalytic reactions with an extended DSMC model. *AIChE J* 2015;61(7):2092–103.

- [15] Mavriplis C, Ahn JC, Goulard R. Heat transfer and flowfields in short microchannels using direct simulation Monte Carlo. *J Thermophys Heat Transf* 1997;11(4):489–96.
- [16] Liou WW, Fang Y. Heat transfer in microchannel devices using DSMC. *J Microelectromech Syst* 2001;10(2):274–9.
- [17] Mädler L, Lall AA, Friedlander SK. One-step aerosol synthesis of nanoparticle agglomerate films: simulation of film porosity and thickness. *Nanotechnology* 2006;17(19):4783–95.
- [18] Mädler L, Kammler HK, Mueller R, Pratsinis SE. Controlled synthesis of nanostructured particles by flame spray pyrolysis. *J Aerosol Sci* 2002;33(2):369–89.
- [19] Kolasinski KW. *Surface science: foundations of catalysis and nanoscience*. 3rd ed. United Kingdom: John Wiley & Sons; 2012.
- [20] Engel T, Ertl G. A molecular beam investigation of the catalytic oxidation of CO on Pd (111). *J Chem Phys* 1978;69(3):1267–81.
- [21] Ladas S, Imbihl R, Ertl G. The reactivity of high oxygen coverages on Pd(110) in catalytic CO oxidation. *Surf Sci* 1993;280(1):14–22.
- [22] Engel T, Ertl G. Elementary steps in the catalytic oxidation of carbon monoxide on platinum metals. In: Eley DD, Pines H, Weez PB, editors. *Advances in catalysis*, 28. Academic Press; 1979. p. 1–78.
- [23] Burghaus U, Jones IZ, Bowker M. Transient study of carbon monoxide oxidation on Pd(111) and Pd(110). *Surf Sci* 2000;454(1):326–30.
- [24] Jones IZ, Bennett RA, Bowker M. CO oxidation on Pd(110): a high-resolution XPS and molecular beam study. *Surf Sci* 1999;439(1):235–48.
- [25] Bird GA. Perception of numerical methods in rarefied gas dynamics. In: Muntz EP, Weaver DP, Capbell DH, editors. *Rarefied gas dynamics: theoretical and computational techniques*, international symposium, 16th, Pasadena, CA, July 10–16, 1988. American Institute of Aeronautics and Astronautics, Inc.; 1989. p. 211–26. Technical Papers.
- [26] Guo X, Yates JT Jr. Dependence of effective desorption kinetic parameters on surface coverage and adsorption temperature: CO on Pd (111). *J Chem Phys* 1989;90(11):6761–6.
- [27] Kołasiński KW, Cemič F, de Meijere A, Hasselbrink E. Interactions in co-adsorbed CO+ O₂/Pd (111) layers. *Surf Sci* 1995;334(1–3):19–28.
- [28] Kołasiński KW, Cemič F, Hasselbrink E. O₂/Pd (111). Clarification of the correspondence between thermal desorption features and chemisorption states. *Chem Phys Lett* 1994;219(1–2):113–17.
- [29] Matveev AV, Sadovskaya EM, Bryliakova AA, Gorodetskii VV. Isotopic transient kinetic study of CO oxidation on Pd (1 1 0). *J Mol Catal A: Chem* 2016;420:18–25.
- [30] Kisliuk P. The sticking probabilities of gases chemisorbed on the surfaces of solids. *J Phys Chem Solids* 1957;3:95–101.
- [31] Kisliuk P. The sticking probabilities of gases chemisorbed on the surfaces of solids—II. *J Phys Chem Solids* 1958;5:78–84.
- [32] Creighton JR, Tseng F-H, White JM, Turner JS. Numerical modeling of steady-state carbon monoxide oxidation on platinum and palladium. *J Phys Chem* 1981;85(6):703–8.
- [33] Guo X, Hoffman A, Yates Jr JT. Adsorption kinetics and isotopic equilibration of oxygen adsorbed on the Pd(111) surface. *J Chem Phys* 1989;90(10):5787–92.
- [34] Sun ZX, Tang Z, He YL, Tao WQ. Proper cell dimension and number of particles per cell for DSMC. *Comput Fluids* 2011;50:1–9.